Engineering and Technology Journal e-ISSN: 2456-3358

Volume 09 Issue 05 May-2024, Page No.- 4161-4171

DOI: 10.47191/etj/v9i05.37, I.F. – 8.227

Static, Rigid Dynamics and Computational Fluid Dynamic Simulation of a Zero Co_2 and Zero Heat Pollution Compressed Air Engine for the Urban Transport Sector

Ngang Tangie Fru[1], Kom K. Yvan Armel[2], Nebo K. Yohan Arnold[3], Biyeme Florent[4], Kanmogne Abraham[5]

[1,2,3,4,5]Department of Mechanical and Industrial Engineering, National Advanced School of Engineering (ENSPY) University of Yaounde 1, Cameroon

ABSTRACT: This article presents major findings created during a research work for sustainable solutions towards the ozone layer depletion and global warming in the name of modeling and simulating a zero CO_2 and zero heat pollution compressed air engine adapted for cities in the Tropics like Cameroon. The static, dynamic and fluid dynamic simulations of the engine conceptual models; products of kinematic and dynamic analyses of the engine realized earlier, led to the adoption of the best engine model for the considered output expectations. This model has $r_3 = 0.177\text{m}$ for $r_2 = 0.054\text{m}$ which was set thanks to how the model proved its resistance to extreme static, rigid movements and fluid solicitations. The method used in this work gives room for some flexibility in the designing process of the engine considering it is a systemic transition from expected values to end internal dimensions of the final model.

KEYWORDS: compressed air engine, kinematics, dynamics, model, simulation

1. INTRODUCTION

The effects of the depleting nature of the ozone layer and the global warming phenomena are not myths in these modern times. According to the State of Global Air 2019, air pollution is the 5th leading risk factor of premature death in a Tropical Country like Cameroon (Institute, et al., 2019). This purge of what is the most beautiful planet of the Milky Way Galaxy cannot be under looked by the scientific world (Morrisette, 1995). This applies to especially engineers, considered custodians of the added value principle, who in general have the major blame to bare here (International Energy Agency, 2009). This research work introduces us to a new area of study that contributes sustainable solutions for ozone layer depletion and global warming.

The simulation of a zero CO_2 and zero heat pollution compressed air engine principally adapted for the cities in the Tropics like Cameroon will be a significant step towards generating contextualized solutions to this climate change calamity (Ngang Tangie Fru, 2019). This research work is not just all about terminating the use of other energy forms in the transport sector but it is about assuring their more sustainable use. This article demonstrates how a more appropriate compressed air engine model is created from a set of conceptual models. The simulation of these engine models considers prior studies on the engine that created feasible conceptual designs which are later on streamlined to a unique functional design following static, rigid dynamic and fluid dynamic simulations of the engine.

2. METHOD AND MATERIALS

This article starts with a dynamic analysis of the engine model formulated earlier in the research (Ngang T. Fru, 2022), this studies led to the establishment of the dimensions of some major volumes. After which was the dynamic analysis and the creation of four 3D models of the engine on SolidWorks with relative $r_2 : r_3$ radi dimensions that fall within the interval; $0.1r_3 \leq r_2 \leq 0.4r_3$ as stated in (Ngang T. Fru, 2022). The simulations realised on ANSYS involve static, dynamic and fluid dynamic simulations. The simulated results discussed in this article are the best results generated from simulating all four acceptable models of the engine. They establish the static, dynamic and fluid dynamic simulations based on the functional expectations of the engine design. These functional expectations include;

- Maximum torque: 130Nm
- Maximum speed: 6000rpm
- Maximum power: 71kW
- Minimum exploitable speed: 4400rpm
- Flywheel radius $R_{fw} = 0.3095\text{m}$

We considered these properties as output properties of our engine with the availability of a 30MPa compressed air supply tank (Verma, 2008). The engine is considered to steadily receive a continuous supply of 10MPa compressed air. The air supplied directly from the tank has a steady temperature of 20℃ with the atmospheric temperature 25℃ and pressure 100kPa.

3. DYNAMIC ANALYSIS

3.1. Dimensioning of Volumes

These calculations concentrate only on the quasi-static volume V_2 (volume of the reception chamber) and, the initial and final dynamic volumes of the expansion chamber (V_5 and V_6).

The following formulae were established for the input force acting on the wings of the combustion chamber.

$$\zeta_1 = p_3 \cos(\theta - \varphi) - q_4 \sin\varphi + \frac{M_3{}^{i} + p_3 r_3 \cos(\theta - \varphi)}{r_3} \quad \textbf{1}$$

$$\Rightarrow f_1 = \frac{2p_4 + (-q_4 - \zeta_1 \sin\varphi)\tan\varphi - \zeta_1 \cos\varphi}{2} \quad \textbf{0}$$

Consider the instances when $\theta = \pi/2$ or $3\pi/2$, $\varphi = \frac{\pi}{2}$, which are moments when the weights of the moving parts are considered negligible we deduce the following;

$$f_1 = p_4 \approx \frac{T_{rot}}{6R_{fw}} \quad \textbf{3}$$

Where $T_{rot} =$ is the expected torque generated by a wing and $R_{fw} =$ the radius of the flywheel of Toyota 115 engine that acts as the output gear of this engine

If we consider that;

$$V_{6min} \approx r_2{}^3 \quad \textbf{4}$$

then from 3 and 4 above,

$$r_2 = \sqrt[3]{\frac{f_1 \sin\theta}{P_6 \ln\frac{P_5}{P_6}}}$$

Thus $$r_{2max} = \sqrt[3]{\left|\frac{f_1}{P_6 \ln\frac{P_5}{P_6}}\right|} \quad \textbf{5}$$

Remember that $0.1r_3 \leq r_2 \leq 0.4r_3$

$$\Rightarrow\gg 2.5\, r_2 \leq r_3 \leq 10 r_2$$

Consider V_2 (volume of the reception chamber) as the volume of a segment of a sphere with height $h_{rc} = 0.618\, r_{rc}$ thus the volume of this hemisphere is;

$$V_2 = 0.30325\, r_{rc}{}^3 \quad \textbf{6}$$

But $V_2 = 6V_5 = \frac{6P_6V_6}{P_5}$ thus

$$\Rightarrow r_{rc} = 2.705\, r_{2max}\sqrt[3]{\frac{P_6}{P_5}} \quad \textbf{7}$$

After considering the above stated values for the independent variables, we can deduce the following dimensions for the principal dependent variables.

Table 1: Acceptable internal Dimensions of Engine before simulation

№	Dependent variables	Values
1	f_{1max}	71N
2	r_{2max}	0.054m
3	V_6	$1.575 \times 10^{-4}m^3$
4	r_{rc}	0.032m
5	V_2	$9.937 \times 10^{-6}m^3$
6	r_{3min}	0.135m
7	r_{3max}	0.54m
8	h_{rc}	0.02m
9	V_5	$1.656 \times 10^{-6}m^3$

4. BILL OF MATERIALS AND 3D PICTURE OF THE COMPRESSED AIR ENGINE

The bill of materials presented in the table below, further subdivides the engine into 13 distinct component parts.

Table 2: Bill of materials

ITEM NO.	PARTS	MATERIALS	QTY.
1	Chassis	Gray Cast Iron	1
2	wings	AISI Type 316L Stainless Steel	6
3	Inlet Manifold	Gray Cast Iron	1
4	Rotor shaft	AISI 4130 Steel, normalized at 87deg. C	1
5	Rotor bearings	Gray cast iron	1
6	Rotor cylinder	AISI Type 316L stainless steel	1

8	Outlet Manifold	Gray Cast Iron	1
9	Hexagon Nut ISO M10	AISI 4130 Steel, normalized at 87deg.C	6
10	Hexagon Bolts ISO M10	AISI 4130 Steel, normalized at 87deg.C	6
11	Timer	Gray Cast Iron	1
12	Reception Chamber Cover	AISI Type 316L stainless steel	1

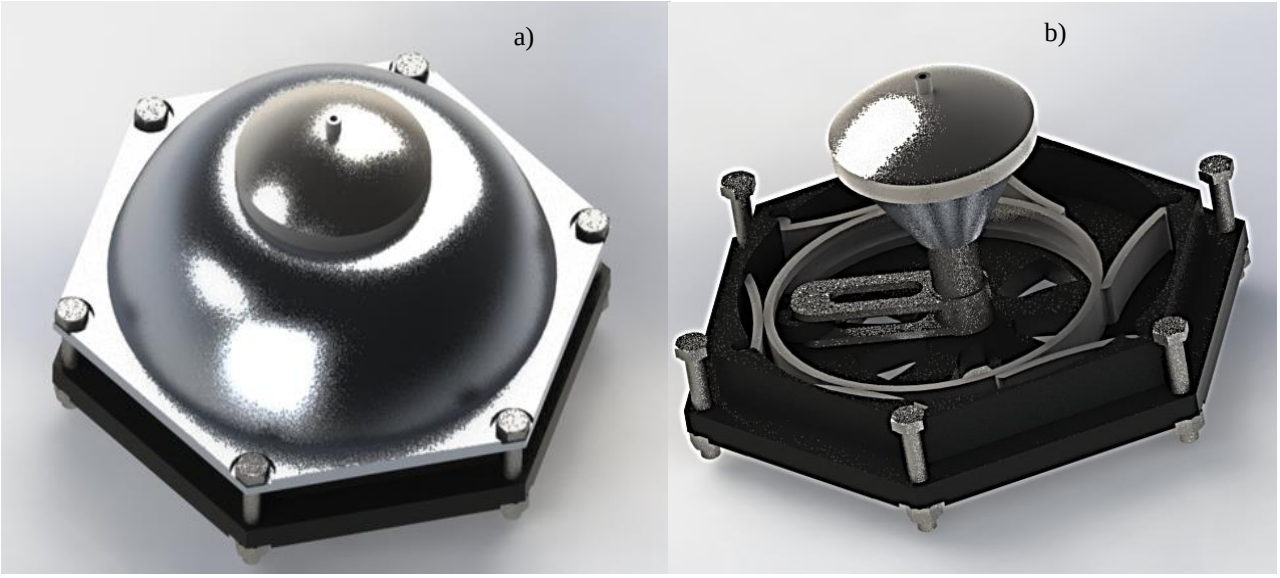

Figure 1: Assembly views with material on SolidWorks a) Full assembly; b) Top opened assembly

5. SIMULATION AND RESULTS

In other to realize computerized simulations, we realized four different 3D models of the engine on SolidWorks 2017. We built these models base on varying dimensions of the rotor shaft. These variations followed the agreed interval of valid r_2 with respect to a fixed value of r_3 from the kinematics studies carried out earlier. In an attempt to reduce the number of recalculations required for the creation of each model, fix r_2 at its maximum value as per the expected output of the engine while r_3 varies between 0.177m and 0.214m. The results discussed in this article are only the acceptable results generated.

5.1. Static Structural Simulations

The structural simulation was on ANSYS 2022 and this involved the following boundary conditions:

- A surface pressure of 30MPa
- Fixed at the Chassis
- Bolt – pretensions 2500N

Because of the complexity of the design, they did the structural simulations in three separate decompositions. The materials used for this exercise are all non-linear materials. The model with the most acceptable results had $r_3 = 0.177m$ from which they made the other dimensions and the simulation results of the model depicted in the paragraphs that follow.

5.1.1 Static structural simulation of the Expansion Chamber

The walls of the chassis, inlet manifold, outlet manifold, rotor cylinder and wings normally surround the expansion chamber. Due to the influential role to be played by the rotor shaft and rotor bearings on the rigidity of the rotor cylinder, this exercise included the latter two, the cylinder, wings and chassis. The inlet and outlet manifolds were not included to reduce the complexity of the decomposition (J.E.R. Costa, 1996).

Trails in this simulation tested the following under a solicitation of 30 MPa and fixed supports at the chassis and the rotor shaft;

i. The resistance of chassis – wings assemble to the surface pressure solicitation;
ii. How well the wings, cylinder, bearing and rotor shaft assembly, dampen the reaction force resulting from the application of the maximum surface pressure on the wings.

i. Chassis – wings assembly

General observations indicated the chassis – wings assemblies always had the minimum-recorded deformations even on solicitation pulses that showed largest deformations on other component parts.

ii. Wing – cylinder – bearing – rotor shaft assembly

Hear the simulation was a little challenging and so for that reason, they recreated an almost instantaneous scenario. This scenario depicts the moment the centers of the shaft, bearing,

and a wing align forcing the wing to close giving room for the injection of compressed air in a semi-confined space. This makes sure the engine has the ability to harvest the highest initial torque from the compressed air. Two circumstances of the deformation of the wing included here were; wing deformation in the absence of the rotor shaft and bearing, and the second considering their presence. Take a glance of the first circumstance below.

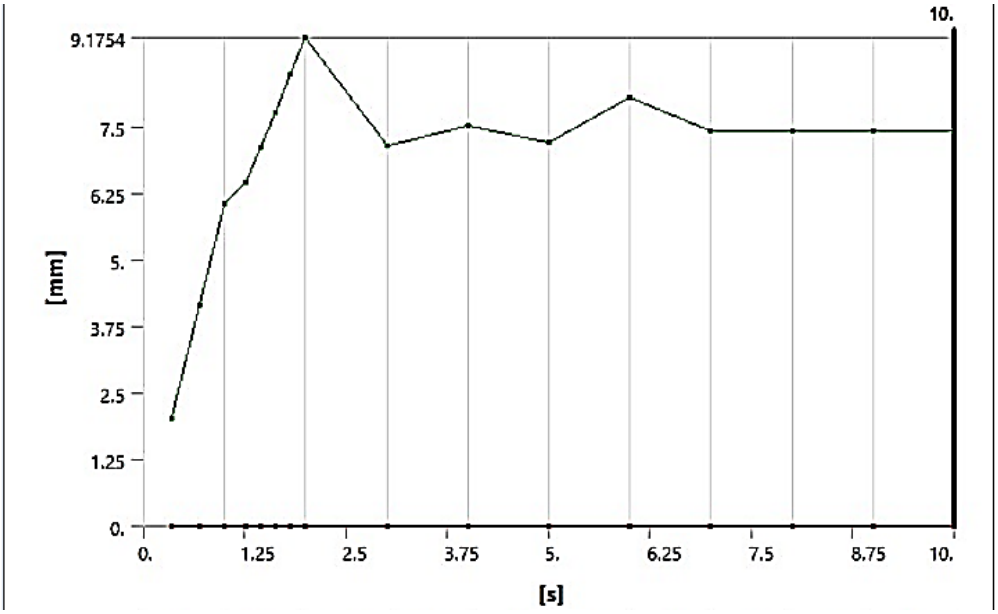

Figure 2: Deformation Vs Time (Rotor shaft and bearing absent)

A node around the maximum deformation regions of the solicited wing as seen here to attain a maximum deformation of 9.1754mm when solicited and it stabilizes at 7.5mm after discharging the solicitation. This implies a distortion of the wing in question.

The second circumstance involves the rotor bearing and shaft.

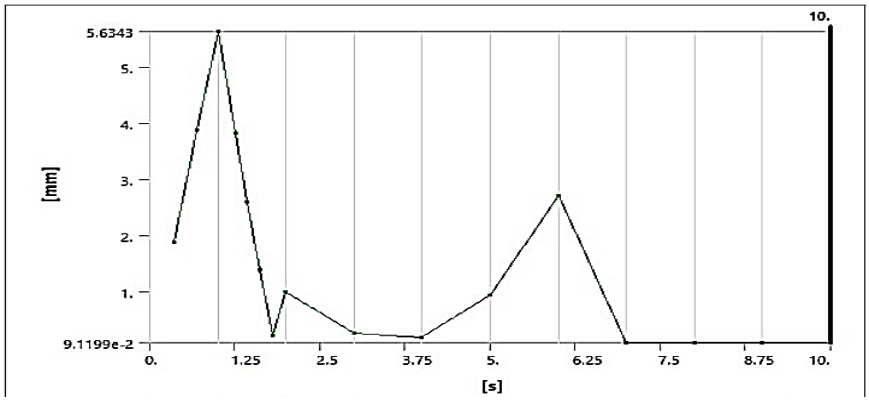

Figure 3: Deformation Vs Time (Rotor shaft and bearing involved)

Here a maximum deformation 5.6343mm as seen here almost half of that seen earlier, what's more intriguing is the fact that the wing gets back to rest after the solicitation is discharged. These finding depicts the effectiveness of this assembly for absorb the instantaneous shock it will receive at the first microseconds of compressed air injection.

5.1.2 Static structural simulation of the Expansion Chamber

The chassis, rotor cylinder, and inlet and outlet manifold encloses the expansion chamber. We also normally find the rotor shaft and bearings as part of this chamber, but for analytical purposes, the chamber was reduced to the inlet manifold, chassis and outlet manifold all held in place by the bolts and nuts. This analysis has as purpose to examine the mechanical strain of the inlet and outlet manifold and to know the needed pretension and strength of the bolt. The principal solicitations used here were 30 MPa surface pressures and 9000 N pretension on the bolt, and assembly fixed at the level of the chassis. In the paragraphs below are the results of this analysis.

i. **Outlet manifold – chassis – inlet manifold assembly**

This assembly witnessed no significant deformation throughout the solicitations. The photo below that depicts the

maximum deformation; only the inlet manifold witnessed a minor deformation just around the positions of attachment that indicates rigidity of the assembly to escapes of fluids during expansion. This implies assembly will be sealed at a pretension of 9000 N.

ii. Bolt –nut assembly

The bolt – nut assembly becomes a point of interest for the bolt is subdued to a maximum deformation of 0.27161mm. For that reason, they selected a node from an area of maximum deformation and an analysis realized to study its deformation with time.

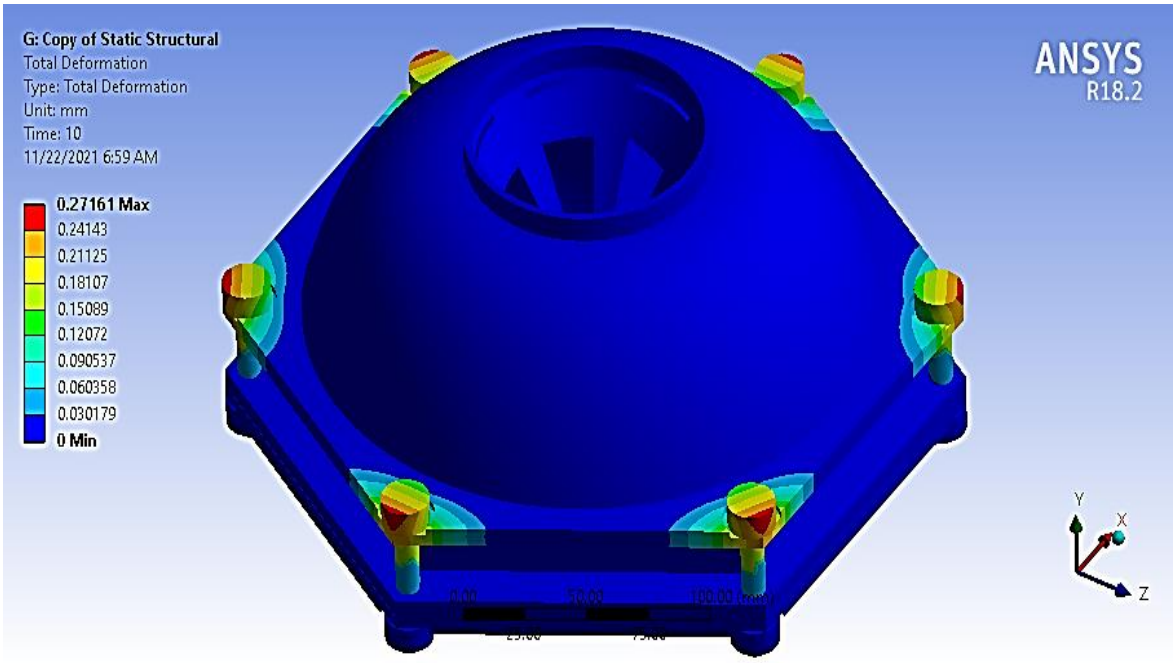

Figure 4: Deformation of Exhaust Chamber

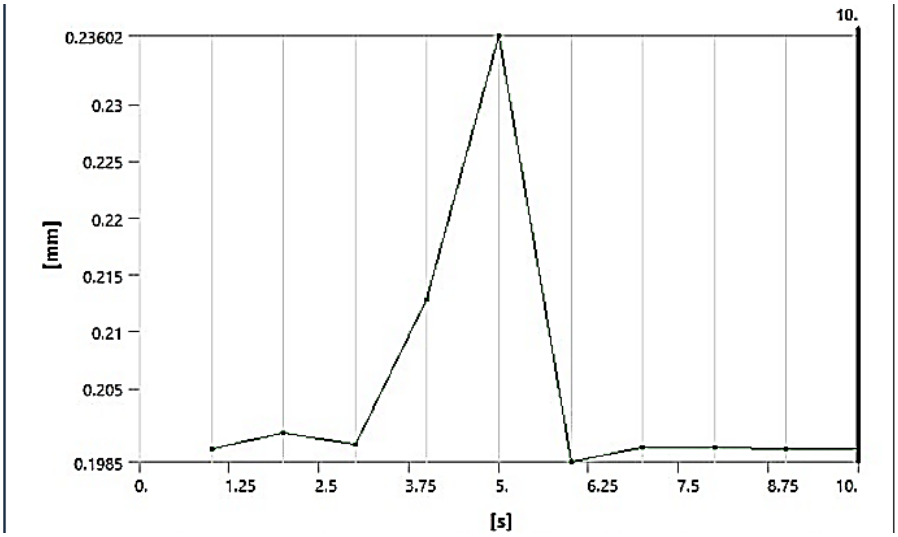

Figure 5: Deformation Vs time (node at bolt area with max deformation)

From this graph, one would see that the bolt remains permanently deformed by 0. 0.1997mm, this is actually due to the applied pretension of 9000 N. But when it witnesses an additional solicitation due to the 30 MPa surface pressure on the walls of the chassis, inlet and outlet manifolds, its deformation spikes up to precisely 0. 0.23602mm but at the discharge of this pressure, it returns almost immediately to its stable position. That is, the resilience of the bolt M10 to the maximum expected solicitation.

5.1.3 Static structural simulation of the Reception Chamber

A cover seals the reception chamber, the inlet manifold and the timer. This analysis was restricted to just the cover and the inlet manifold assembly. The goal of the analysis was to test the resistance of this enclosure to the 30 MPa surface solicitations and to recheck to guarantee the large deformation registered at the inlet manifold was not from the 30 MPa surface pressures but just the bolt pretension. They

fixed the assembly as such at just the bolt bores of the inlet manifold.

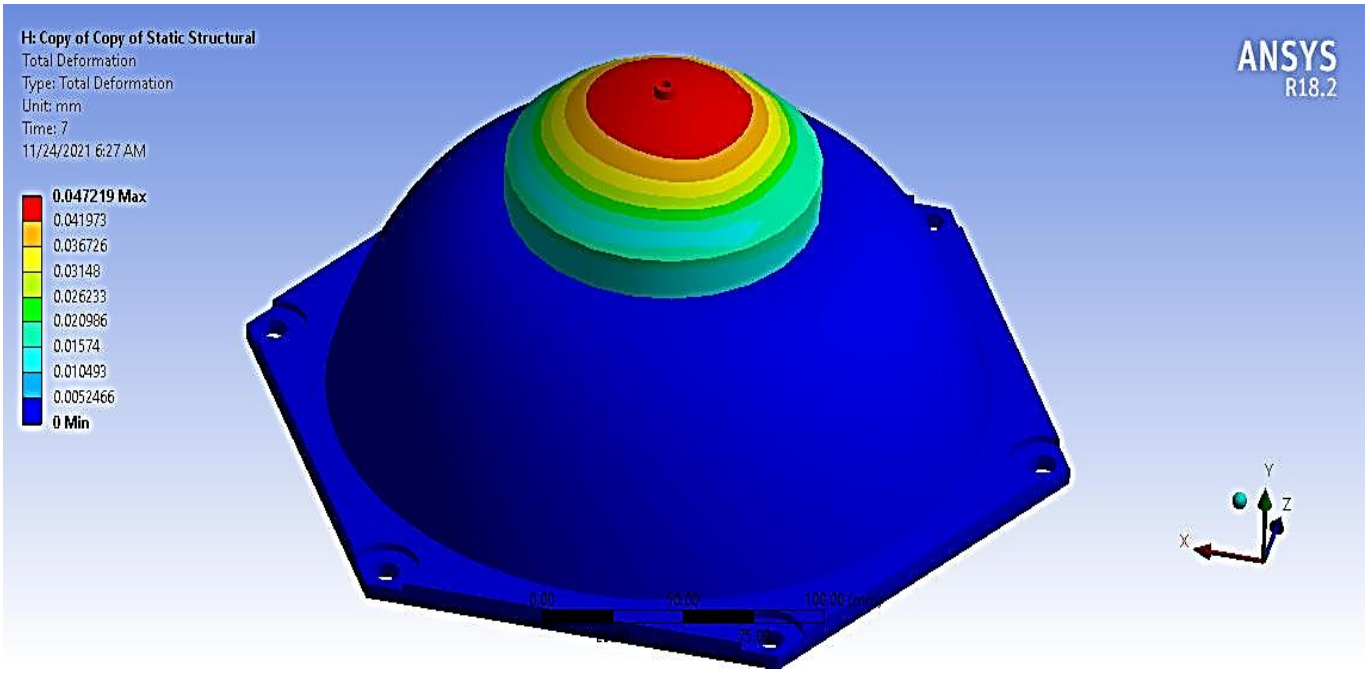

Figure 6: Deformation of Reception Chamber

From the findings above, one can quickly realize the deformation range is small; from 0mm to 0.047219 mm. This is almost insignificant but because the cover records the largest deformation in the assembly, they selected a node from an area with largest deformation and the deformation sketched in a graph for clearer review of the findings. The inlet manifold here records the lowest deformation thus, confirmation the deformation recorded earlier came from the pretension of the bolts.

As can be seen in the graph bellow, the selected node clearly demonstrates on the graph that it will regain its initial position with the discharge of the solicitation, another big plus for the design as a whole.

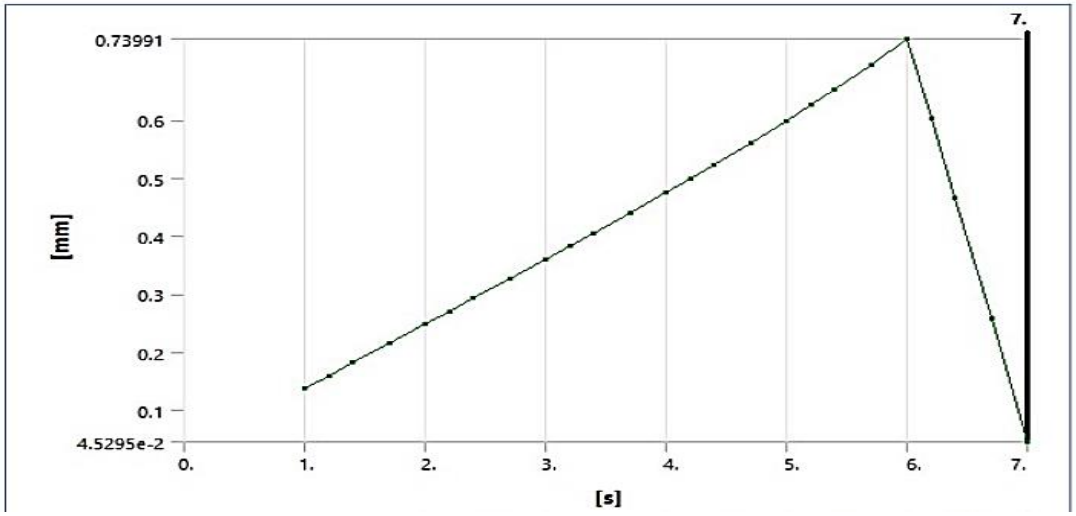

Figure 7: Deformation Vs time (node at cover area with max deformation)

5.2. Rigid Dynamics Simulations

Carrying out the rigid dynamic simulations entails the use of some major input loads (Wang, et al., 2022). These loads are summarized in the below;

- Maximum torque: 130Nm
- Maximum speed: 6000rpm/ 100rps/

With the above considerations, an interpretation of rigid dynamics simulation of the engine was as follows.

5.2.1. Rigid dynamic simulation input loads

In an attempt to represent the simultaneous momentary expansion of gases in the various expansion chambers, moment forces where allocated at the various wing

connection joints. These forces had the following proprieties per wing;

- Period of 0.01s,
- Amplitude 130Nm
- Phase varying from 0 to 75°,
- Cosine shape

Thus, the following formulations for each input moment;

- For wing 1; $130 \times \cos^{20}(\text{time} \times 90°/0.01)$
- For wing 2; $130 \times \cos^{20}((\text{time} \times 90°/0.01) - 15°)$
- For wing 3; $130 \times \cos^{20}((\text{time} \times 90°/0.01) - 30°)$
- For wing 4; $130 \times \cos^{20}((\text{time} \times 90°/0.01) - 45°)$
- For wing 5; $130 \times \cos^{20}((\text{time} \times 90°/0.01) - 60°)$
- For wing 6; $130 \times \cos^{20}((\text{time} \times 90°/0.01) - 75°)$

Figuratively we had the following inputs;

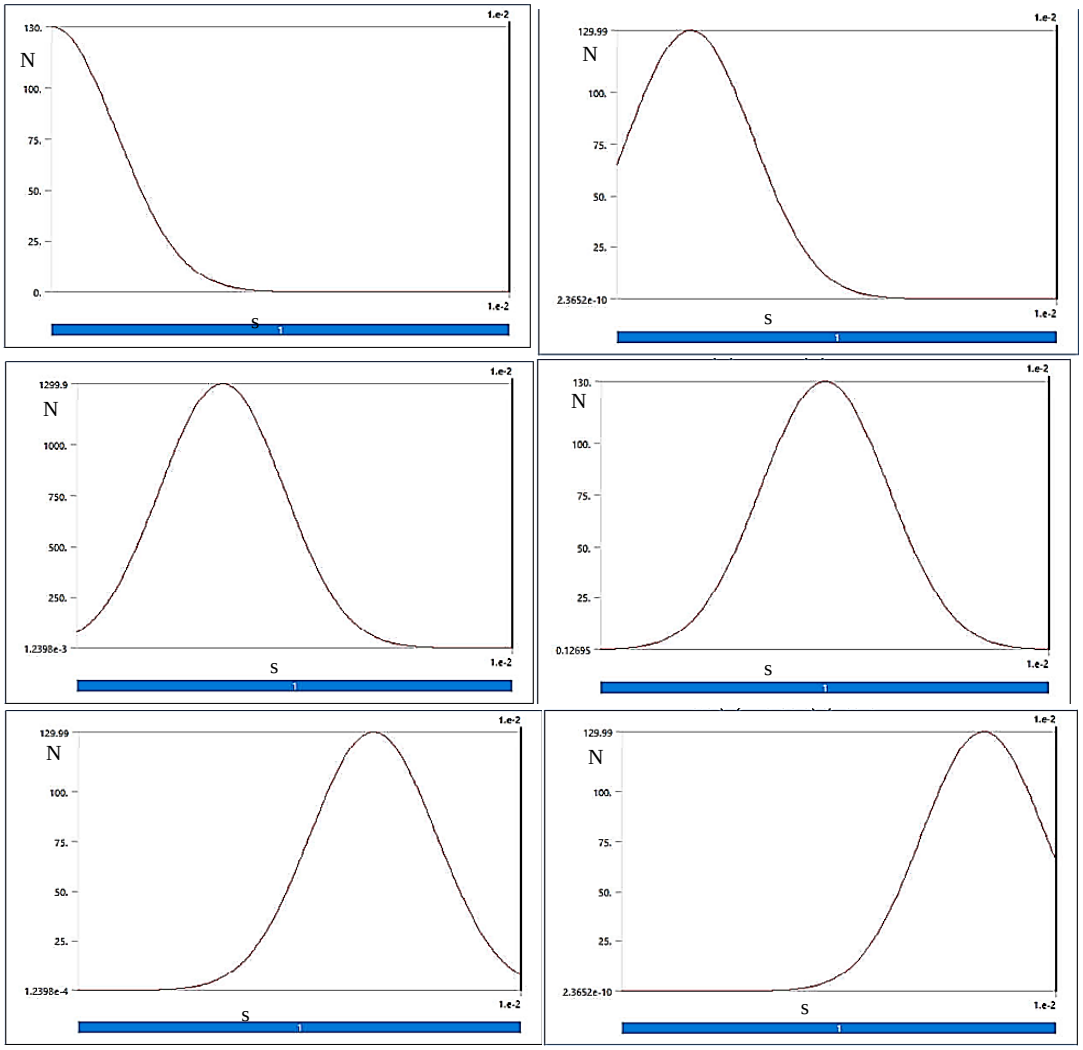

Figure 8: Input moments for rigid body dynamics simulation

i. Rigid dynamic simulation energy results

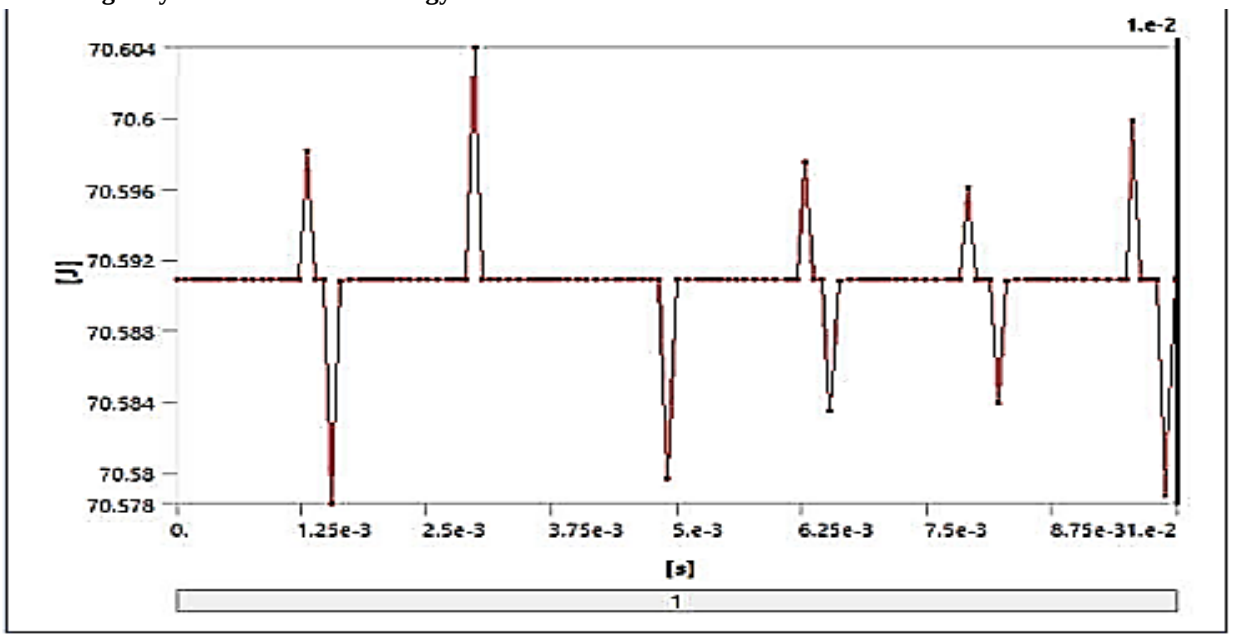

Figure 9: Energy results of the rigid dynamics simulation from wing 1

Attaching an energy probe on the rotor shaft, gave the graph above which displays and almost stable energy generation throughout a complete rotational cycle of the rotor shaft. The maximum deviation is as low as ± 0.05 J, which indicates that 70.59J of energy, is almost stable throughout the engine operation.

ii. Rigid dynamic simulation moment results

A joint probe attached to the rotor, generated a continuous positive total moment in one complete cycle. The total moment appears to be over 60 folds of the minimum at some instances. The total moment seen in purple, shortly spikes to 941.69Nm about midway through the cycle. This means the main moment contributor (in green) is about the rotational axis of the rotor. The purple plot represent the total moment.

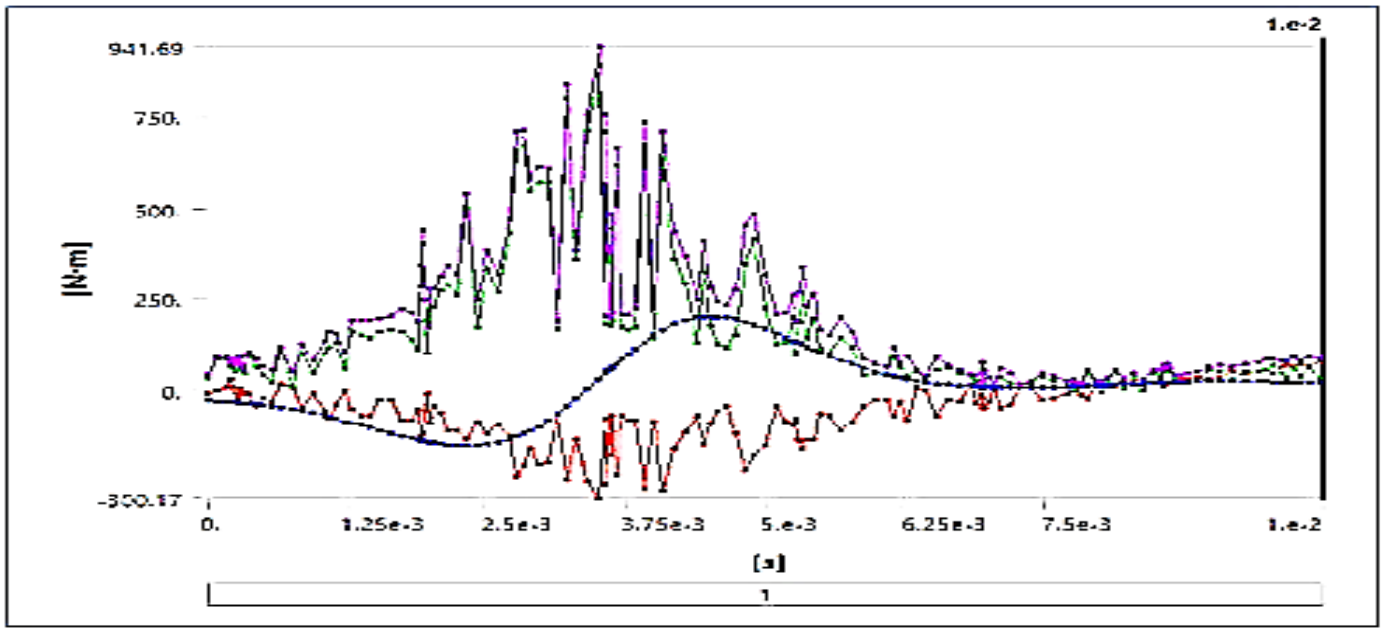

Figure 10: Moment at the Rotor Shaft

5.3. Computational Fluid Dynamics Simulations

We carried out this simulation to check flow of compressed air throughout the different conduits in an attempt to guarantee the presence of compressed air at their various destinations (Singh, et al., 2012). We studied principally two sets of inlet – outlet pressures here; one to depict the highest possible supply pressure and the second the lowest possible

supply pressure. The paragraphs that follow represent our findings so far.

5.3.1. Flow with maximum supply pressure

Considering a supply pressure of 30MPa, we saw that compressed air would glide through the conduit into the expansion chamber. We find this in the velocity contour below, as there is some displacement at the lower end of the expansion chamber

.

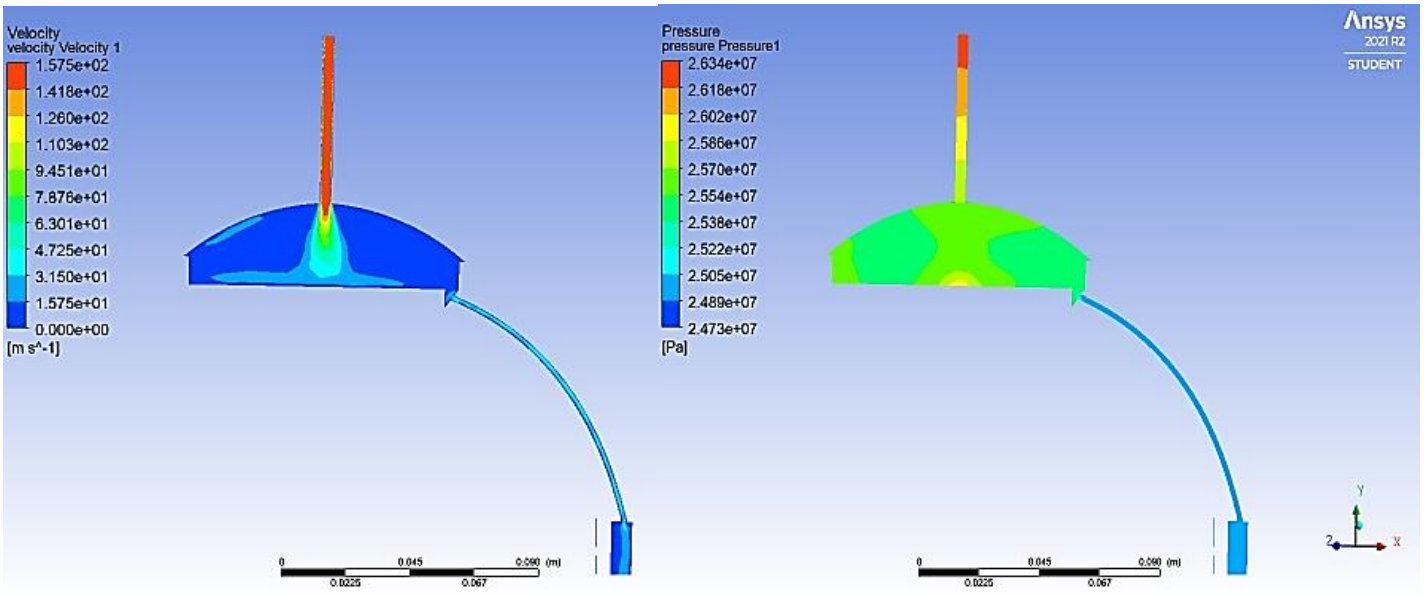

Figure 11: Velocity and pressure contour of input flow at maximum supply pressure

The pressure contour displayed an almost even distribution of the fluid's pressure across the stipulated pressure gradient.

5.3.2. Flow with minimum supply pressure

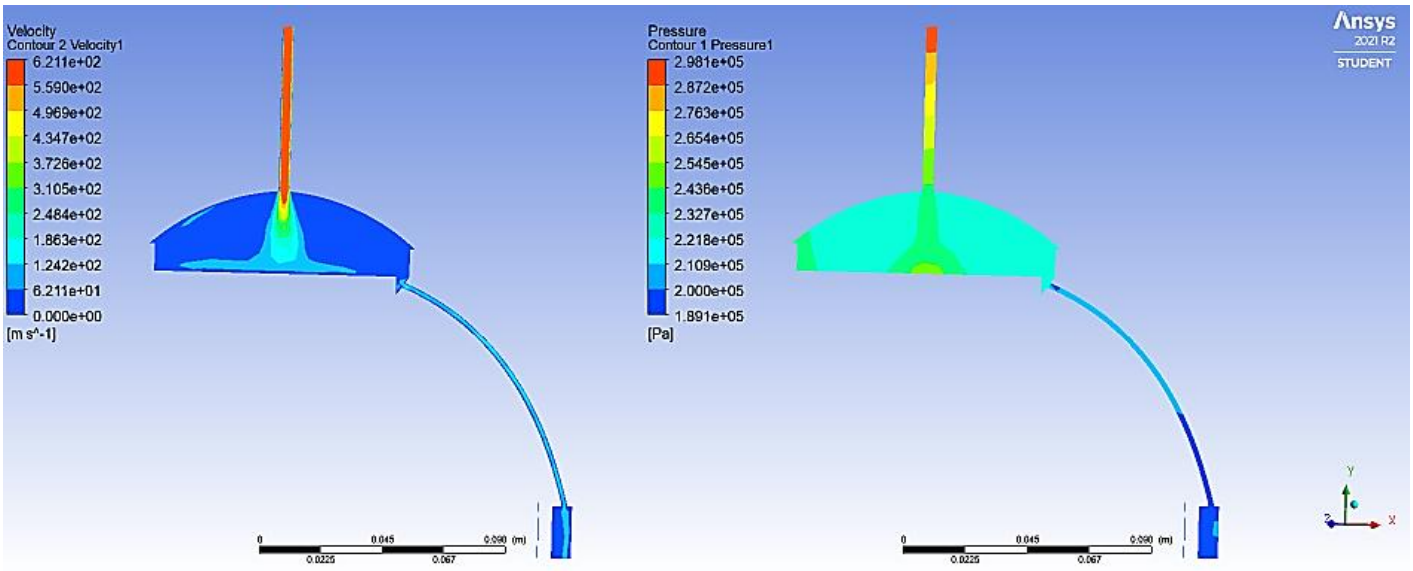

Figure 12: Velocity and Pressure Contours of Input at minimum supply pressure

We considered a supply pressure of 5bars for this analysis. Though this is over 60 times less than the maximum, it was to guarantee the dexterity to pressure variations of the input conduit assembly. We can identify some flow from the inlet down to the expansion chamber in the velocity contour and an almost linear distribution of the pressure over the selected pressure gradient.

CONCLUSION

Conclusion drawn from the simulation results above demonstrate that the most acceptable design of this engine

will need to have r_3 = 0.177m for $r_2 = 0.054$m . Thus for any additional analysis of the Zero CO2 and Zero Heat Pollution Compressed Air Engine design with the following expectations for an input energy source of 30MPa and a steady supply of 10MPa for maximum output, the internal dimensions of the engine will need to be fixed as follows;

Table 3: Internal dimensions of engine after simulation results

№	Dependent variables	Values
1	f_{1max}	71N
2	r_{2max}	0.054m
3	V_6	$1.575 \times 10^{-4}m^3$
4	r_{rc}	0.032m
5	V_2	$9.937 \times 10^{-6}m^3$
6	r_3	0.177m
7	h_{rc}	0.02m
8	V_5	$1.656 \times 10^{-6}m^3$

The simulation of the internal forces this engine reduced the number of acceptable models from four to one model. The above dimensions could be simulated further to develop the external dimensions of the engine which is essential for the development of the engine prototype.

REFERENCES

1. Albritton, D., 1998. What Should Be Done in a Science Assessment In Protecting the Ozone Layer: Lessons, Models, and Prospects, s.l.: ResearchGate.
2. Angell, J. K. & Korshover, J., 2005. Quasi-biennial and Long-term Fluctuations in Total Ozone. Monthly Weather Review vol. 101, p. 426–443.
3. Craig, K., 2011. Fundamental Principles of Mechanical Designs. s.l., s.n.
4. Department of Climate Change Australia, 2008. National Greenhouse Gas Inventory (2006). s.l.:Australian Government.
5. Fergusson, A., 2001. Ozone layer Depletion and Climate Change: Understanding the linkage. Canada: Minister of Public Works and Government Services Canada.
6. Institute, H. E., Columbia, U. o. B. & Evaluation, I. f. H. M. a., 2019. State of Global Air/ 2019. [Online] Available at: www.stateofglobalair.org [Accessed 2019].
7. International Energy Agency, 2009. Transport, Energy and CO2. Directorate of Sustainable Policy and Technology.
8. J.E.R. Costa, B. C., 1996. Static and Dynamic Simulation in the Classical Two-Dimensional Anisotropic Heisenberg Model. The American Physical Society, 54(2), pp. 994-1000.
9. K., M. M., P.Rathod, D. & Arvind S., P. S., 2012. Study and Development of Compressed Air Engine Single Cylinder: A Review Study. International Journal of Advanced Engineering Technology, pp. 271-274.
10. K.T. Chau, 2014. 21 - Pure electric vehicles. In: Alternative Fuels and Advanced Vehicle Technologies for Improved Environmental Performance. s.l.:Woodhead Publishing, p. 655 – 684.
11. Kahn, B., 2016. World's Atmospheric Carbon Dioxide Passes 400 PPM Threshold. Permanently. Climate Central, 27 September.
12. Kavalec, C., 1999. Vehicle choice in an aging population: Some insights from a stated preference survey from California. The Energy Journal, pp. 20(3), 123-138.
13. Kronberg, N. & Shawn, W., 2019. Transport Statistics Great Britain. Department of Transport.
14. Morrisette, P. M., 1995. The Evolution of Policy Responses to Stratospheric Ozone Depletion. Natural Resources Journal, p. Vol 2.
15. Ngang T. Fru, N. K. K. A. B. F., 2022. Modeling of a Zero CO2 and Zero Heat Pollution Compressed Air Engine for the Urban Transport Sector. Mechanical Engineering Research, Vol. 10, No. 1(2022), pp. 25-34.
16. Ngang Tangie Fru, 2019. Zero CO2 and Zero Heat Pollution Compressed Air Engine for the Urban Transport Sector, Yaounde Cameroon: University of Yaounde 1.
17. Ngang, T. F., 2019. Zero CO2 and Zero Heat Pollution Compressed Air Engine for the Urban

Transport Sector, Yaounde Cameroon: University of Yaounde 1.

18. Rucks, J. W. a. G., 2015. 5 steps to an urban transportation revolution. GreenBiz, 17 March.
19. Singh, K. D. et al., 2012. Computational Fluid Dynamic Modeling of Industrial Flares Operated in Stand-By Mode. Industrial & Engineering Chemistry Research, pp. 1-35.
20. Sivasakthivel, T. & K.K. Siva, K. R., 2011. Ozone Layer Depletion and Its Effects: A Review. International Journal of Environmental Science and Development.
21. Thipse, S., 2008. Compressed Air Car. Engine Development Laboratory: s.n.
22. Thompson, A., 2016. August Declared Hottest on Record: NASA. Climate Central, 14 September.
23. Verma, S., 2008. Air Powered Vehicle. The Open Fuels & Energy Science Journal, pp. 54-56.
24. Wang, X. et al., 2022. Dynamic Modeling and Simulation of rigid-flexible coupling cable system by absolute nodal coordinate formulation. Scientific Reports, pp. 1-14.